Automatic estimation of kinetic and isotherm parameters from ZLC experiments

Automatic estimation of kinetic and isotherm parameters from ZLC experiments

Daniel Friedrich*, Enzo Mangano, Stefano Brandani

School of Engineering, University of Edinburgh, Edinburgh EH9 3JL, UK

d.friedrich@ed.ac.uk

Abstract

In order to automate and improve the analysis of the experimental Zero Length Column (ZLC) data a general adsorption simulator is applied to the simulation of the ZLC system. The output of this ZLC simulation is linked to a hybrid optimisation strategy: combining a global Genetic Algorithm (GA) with a local Nelder-Mead algorithm ensures an efficient and accurate optimisation procedure. By minimising the deviation between the experimental data and the simulation the kinetic and equilibrium parameters of the adsorbent can be estimated. In the first step the parameters of the blank experiment are fitted; thus taking the dynamics of the detector and the system piping into account. In the second step several experiments at different flow rates and temperatures are fitted simultaneously. This increases the accuracy and reliability of the results. The automated parameter estimation was applied to ZLC runs with carbon dioxide on zeolite 13X pellets. The results agree with the traditional analysis methods and with independent measurements. In addition it is demonstrated that it is possible to approximate the correct adsorption isotherm from ZLC runs under kinetic control. The automatic analysis tool allows the inclusion of nonlinear effects in the fitting and lowers the access barrier to the application of the ZLC method.

Keywords: Zero length column; automated parameter estimation; adsorption equilibrium and kinetics; hybrid optimisation; carbon dioxide; zeolite 13X

1. Introduction

The Zero Length Column (ZLC) method is a well known technique for the measurement of the kinetic and equilibrium properties of adsorption systems. Briefly, in the ZLC method the desorption curve of a small amount of adsorbent previously equilibrated with a known gas mixture is measured. By changing the experimental conditions, i.e. flow rate of the purge gas, the system can be operated under equilibrium or kinetic control; thus equilibrium and kinetic properties can be investigated in the same series of experiments. The reliable measurements for fast and slow kinetics combined with the small required sample quantity (less than 10mg) make the ZLC method a very useful and flexible tool for kinetic and equilibrium measurements for a wide range of materials.

The ZLC technique was first introduced in 1988 by Eic and Ruthven as a novel chromatographic technique to measure intra-crystalline diffusion in small samples of zeolite [1]. The technique has been applied to the determination of the kinetics of systems dominated by intra-crystalline diffusion [2]–[6], macropore diffusion [7], [8] and surface resistance [9]–[11]. Over the years the technique has

been continuously developed with the introduction of different variants of the traditional method such as the tracer ZLC for the measurement of self-diffusivity [12]–[14], the counter-current ZLC for the measurements of counter diffusion [14], [15], and the partial loading ZLC experiment [12], [16], [17]. The technique has been also extended to the measurements of kinetics in liquid systems [15], [18]. The validity of the basic assumptions of the theoretical model have been widely investigated and the simple model has been modified to be applicable for measurements under nonlinear conditions [19], [20], non-isothermal systems [21], for bi-porous adsorbents [22] and for systems with crystal size distribution [23]. The technique, originally invented for diffusion measurements, was successfully applied for measurements under equilibrium control. Under these conditions the equilibrium isotherms can be extracted from the ZLC desorption curves [24], [25]. The results have widely shown the reliability of the technique as well as its flexibility in characterising various adsorption systems. All this establishes the ZLC as an essential tool for the investigation of the adsorption properties of prototype adsorbents [26]. While the experimental technique is well developed the traditional analysis methods still analyse each experimental run separately. However, for kinetic measurements it is crucial to analyse runs with different conditions, i.e. temperature and flow rate, in connection with each other to reach the correct conclusions on the dominating kinetic mechanism [27]. Furthermore, the current analysis methods require significant experience from the operator due to the dynamic nature and large operating range of the ZLC experiments. For this reason, an automated analysis method could lower the access barrier to the application of the ZLC method.

The use of full curve fits of ZLC experiments was first proposed by Micke et al. [28], [29] but the regressions were carried out on individual curves leading to an incorrect apparent concentration dependence of the diffusivity [19]. The first application of the simultaneous regression of multiple ZLC curves was used to interpret the kinetics of methanol on 13X zeolite [13], since for this system it is experimentally difficult to reach pure kinetic control and the accuracy of the traditional long-time asymptote approach is reduced. The same method was used to determine the kinetics of adsorption of carbon dioxide on fragments of a carbon monolith [30]. Other authors have proposed the use of full curve fits [31], [32], apparently unaware of the earlier studies. Han et al. [32] repeated the error of using only single curves and their approach did not give proper weighting to the long-time asymptotic part of the desorption curve which contains most of the kinetic information. Loos et al. [31] did advocate the use of multiple curve fits as previously suggested [13], and included both the effect of the blank dynamics and of crystal size distributions. All the approaches listed above assumed either a linear isotherm or a constant diffusivity (or both), thus obtaining an analytical solution [13], [31], [32] or a convolution integral [28] to interpret the results, thus not allowing for the inclusion of nonlinear effects. This shows that there is a need for full curve fits with detailed adsorption simulations to handle cases with nonlinear effects and arbitrary isotherms.

Here an automated analysis method for the ZLC experiments is presented. This method combines a detailed adsorption process simulator, which takes into account nonlinear and non-isothermal effects, with numerical optimisation methods to automatically estimate both kinetic and equilibrium parameters from multiple ZLC experiments. The use of the automated tool is demonstrated through the estimation of the kinetic and equilibrium parameters of CO_2 adsorption on zeolite 13X from several experimental runs at different flow rates and temperatures.

2. Zero Length Column method

2.1 Zero Length Column experiments

The Zero Length Column is housed in a 1/8 in. Swagelok union in which a small amount (10-15 mg) of adsorbent material is inserted between two sinter discs. The column is placed inside an oven to keep the temperature constant during the experiment. A simplified schematic of the system is shown in Figure 1. The experimental procedure is as follows: first the sample is exposed to a known feed mixture of CO_2 and an inert gas (helium in the case considered here); once the sample equilibrates the inlet flow is switched to the purge gas (pure He) and the output of the column is recorded.
By changing the flow rate and/or temperature the ZLC system can be run in different operational regimes and thus different properties, i.e. kinetic and/or equilibrium, can be measured. Furthermore, a change in the pellet size or the inert gas, i.e. from helium to nitrogen, can be used to investigate the dominant diffusional resistance [8].

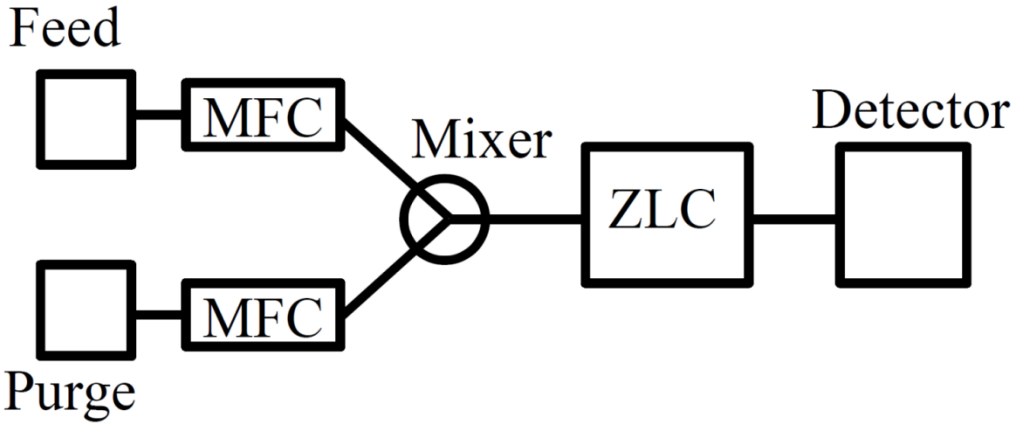

Figure 1: Simplified schematic of the ZLC system. The feed and purge gas pass through Mass Flow Controllers (MFC) before entering the ZLC.

2.2 Traditional analysis of ZLC experiments

The main advantage relative to other chromatographic methods is represented by the very small amount of sample used and the small size of the column. Due to this the external mass transfer resistances can be neglected. In the case of carbon dioxide on 13X under the experimental conditions the column is also isothermal. Furthermore, due to the short length (~9 mm) of the column the relative axial dispersion is large and the system can be effectively treated as a well-mixed cell, for which the mass balance can be written as

$$V_s \frac{d\overline{Q}}{dt} + V_g \frac{dc}{dt} + Fc = 0 \qquad (1)$$

in which V_s and V_g are the volume occupied by the solid and the gas phase inside the column, respectively; $\overline{Q}$ is the average adsorbed phase concentration; c is the gas phase concentration; and F is the volumetric flow rate.

By assuming Fickian diffusion inside spherical particles with diffusivity D and a linear equilibrium isotherm with Henry's constant K the analytical solution for the system is [18]

$$\frac{c}{c_0} = 2L\sum_{n=1}^{\infty} \frac{\exp\left(-\frac{\beta_n^2 Dt}{R^2}\right)}{[\beta_n^2 + (L-1-\gamma\beta_n^2)^2 + L - 1 + \gamma\beta_n^2]} \tag{2}$$

Where β_n are given by the roots of

$$\beta_n \cot \beta_n + L - 1 - \gamma\beta_n^2 = 0 \tag{3}$$

with

$$L = \frac{FR^2}{3KV_s D} \tag{4}$$

and

$$\gamma = \frac{V_g}{3KV_s} \tag{5}$$

The dimensionless parameter L is defined as the ratio between the diffusional time constant D/R^2 and the convective desorption time constant F/KV_s : it is a measure of how far the system is from equilibrium control [11], [33]. When L is small ($L < 1$) the adsorbed phase is essentially at equilibrium with the gas phase and the desorption rate is controlled entirely by convection, while if L is large ($L >> 1$) the process is kinetically controlled. Experiments at different flow rates are needed to prove which regime is controlling the system [24], [25]. The parameter γ is the ratio between the hold-up in the fluid phase and accumulation in the solid; for gaseous system this is generally very small and can be neglected, but it can become significant if the adsorption is relatively weak or in the case of liquid systems [18], [30].

3. Automated parameter estimation tool

3.1 Simulation of the ZLC experiments

The ZLC system is simulated with the in-house adsorption process simulator CySim [34]. The application of a general adsorption simulator allows the inclusion of nonlinear effects in the analysis and, equally important, facilitates the direct use of the resulting parameters in adsorption process simulations without the need for error-prone conversions. The simulator used was originally developed for the simulation of the dual-piston PSA system [35] and later extended to a general adsorption cycle simulator which can be applied to arbitrary adsorption cycles [36], [37]. Briefly, the simulator contains a number of modular units used in adsorption cycles, such as adsorption columns, valves and splitters. These units can be connected in arbitrary ways to simulate a wide range of adsorption processes. The different cycle steps are controlled by opening and closing valves or changing the settings of the mass flow controllers (MFCs).

The process simulation for the ZLC system is built from units representing the separate parts of the system as shown in the schematic in Figure 1. In this representation the ZLC and the surrounding units of the system are explicitly defined. The feed and purge unit on the left side of the schematic define the gas composition and temperature of the feed and purge stream, respectively. For example, all simulations in this contribution are matched to experiments with a feed gas at atmospheric pressure and with 10% CO_2, while the purge gas is pure helium at atmospheric pressure. The two MFCs control the flow rate and are switched to go from the feed step to the purge step. The mixer between the feed and purge line and the column represents the volume of the piping in the real system. Both the ZLC unit and the detector unit are based on the adsorption column unit presented previously [34]. The column unit contains several options for the mass, momentum and energy balances:

1. Mass balance:
    a. Macropore: no macropore, macropore LDF or macropore diffusion
    b. Micropore: micropore equilibrium, micropore LDF or micropore diffusion
    c. Adsorption isotherm: linear, Langmuir or dual-site Langmuir
2. Momentum balance: no pressure drop or pressure drop from the Ergun equation
3. Energy balance: isothermal or non-isothermal operation

This choice in the underlying models allows the testing of the assumptions of the ZLC system, e.g. isothermal operation, and the different mass transfer mechanisms for different adsorbents. In this contribution only different adsorption isotherms are investigated while the momentum and energy balance are fixed at no pressure drop and isothermal operation, respectively, and the kinetic model is fixed at macropore diffusion and micropore equivalent LDF. The governing equations for this case are given by

$$\frac{\partial c}{\partial t}+\frac{(1-\varepsilon)}{\varepsilon}\cdot\frac{\partial \overline{Q}}{\partial t}+\frac{\partial (c\cdot v)}{\partial z}+\frac{\partial J}{\partial z}=0 \tag{6}$$

$$Q=\varepsilon_p c^m+(1-\varepsilon_p)q \tag{7}$$

$$\varepsilon_p\frac{\partial c^m}{\partial t}+(1-\varepsilon_p)\frac{\partial q}{\partial t}+\frac{1}{r^2}\frac{\partial}{\partial r}\left(-D_p r^2\frac{\partial c^m}{\partial r}\right)=0 \tag{8}$$

$$\frac{dq}{dt}=\frac{15D_\mu}{r_\mu^2}\left(q^*-q\right) \tag{9}$$

$$q^*=\frac{q_{s1}b_1^0 Px}{1+b_1^0 Px}+\frac{q_{s2}b_2^0 Px}{1+b_2^0 Px} \tag{10}$$

$$b_i^0=b_i\,exp\left[\frac{-\Delta H_i}{R}\left(\frac{1}{T}-\frac{1}{T_{ref}}\right)\right] \qquad \text{for i=1,2} \tag{11}$$

The detector is modelled as a CSTR with the known volume of the detector. The dynamics of the detector are not known explicitly but the desorption curve of the blank experiment is qualitatively comparable to the desorption curve for a system with a Langmuir isotherm and LDF kinetics. Thus the governing equations for the detector are given by

$$\varepsilon V\frac{dc}{dt}+(1-\varepsilon)V\frac{dq}{dt}=F(c_{in}-c) \tag{12}$$

$$\frac{dq}{dt} = k\left(\frac{q_s bPx}{1+bPx} - q\right) \tag{13}$$

This is the simplest model that accurately reproduces the response on the experimental system. It effectively includes a mixing volume and the existence of “side pockets” which yield a tail in the concentration response. The effective side pockets are accumulation and mixing zones that are in both the lines and the detector. While the components in the lines are accounted for, the actual internal design and flow configuration of the detector are not known a priori and need to be estimated from experimental data. The LDF mass transfer parameter, the saturation capacity and the equilibrium constant of the detector in Eq. 13 are fitted from the blank experimental data.

3.2 Parameter estimation from the ZLC experiments

The automated estimation of the kinetic and equilibrium parameters from the ZLC experimental data is performed by linking the simulation of the ZLC system developed in Section 3.1 to an optimisation routine.

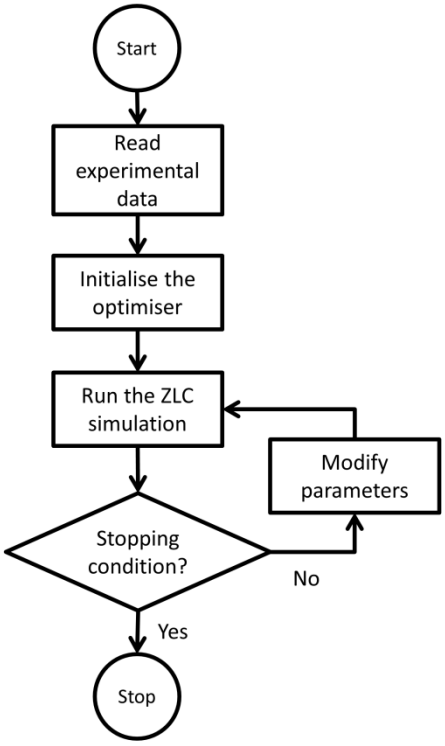

Figure 2: Flowchart for the automated parameter estimation.

The flowchart in Figure 2 gives an overview of this approach. First the experimental data sets are read in and analysed. After this the optimiser is initialised according to the user input and the analysis of the experimental data. Then the ZLC simulations are run with the initial parameter values and the results are compared to the experimental data. If the deviation between the simulations and experimental data is above a certain threshold, the parameters are modified by the optimisation routine with the aim to minimise this deviation and the simulations are run again with the modified parameters. Once the deviation reaches a certain value it is assumed that the fitted parameters

correspond to the true experimental parameters. A further stopping condition is the maximum number of simulation runs which ensures that the program stops even if the deviation can't be minimised. In the next paragraphs these steps are explained in more detail.

After the experimental data is read in this data is normalised and analysed. At the end of each experimental run the CO_2 concentration will go to zero and thus the detector output back to the baseline. Here the baseline is calculated as the average detector output during the last 2 minutes of the experiment and the raw data σ is normalised by

$$C = \frac{\sigma - \sigma_b}{\sigma_0 - \sigma_b} \tag{14}$$

Where σ_b and σ_0 are the baseline and initial value of the experimental data, respectively. From the normalised experimental data the start of the desorption step, i.e. the switch to the purge gas, is calculated as the time when the normalised detector output drops below 0.99. While this procedure might not catch the actual switch time and neglects the gas hold-up in the system the resulting error is minimised due to the treatment of the blank data in the same way.

Next the total adsorbed amount is calculated from the area under the desorption curve [38]

$$q_T = yF\int_{t_0}^{t_1} \frac{C(t)}{1 - yC(t)} dt \tag{15}$$

From this number the value for the blank has to be subtracted to get the correct total adsorbed amount at the start of the experiment. The total adsorbed amount can be used to fix one point on the adsorption isotherm and thus to reduce the number of parameters.

To obtain an initial approximate estimate of the L parameter an exponential function, i.e. a line in the semilog plot, is fitted to the long-time region of the experimental data. From this fit the parameter L and the effective pore diffusivity can be estimated [1], [16]. The parameter L can be approximated as 2 divided by the intercept; this approximation is valid for large L, i.e. $L > 5$. In the kinetically controlled regime, i.e. $L >> 1$, the effective pore diffusivity can be estimated from the slope S by

$$D \approx R^2 \frac{S}{\pi^2} \tag{16}$$

Furthermore, the deviation of the fitted exponential and the experimental data is a good approximation of the noise in the experimental data. This noise level N is calculated as the least squares error between the experimental data and the long-time region fit. The noise level will be used to scale the deviation between the simulation and experiment in the parameter estimation.

After the preliminary analysis of the experimental data the parameter estimation is started. To describe micro- and macropore kinetics and the dual-site Langmuir isotherm 8 parameters are required: 2 for the macropore diffusion and micropore LDF and 6 for the dual-site Langmuir isotherm. These parameters are D_p, D_μ / r_μ^2, q_{si}, b_i and $-\Delta H_i$ (for i=1,2) in Eqs. 8–11. The parameter estimation is set up in a flexible manner so that any combination of these parameters can be fitted while the other parameters are kept constant. For example, the parameters for the second site of the dual-site Langmuir isotherm, i.e. q_{s2}, b_2 and $-\Delta H_2$ in Eqs. 10 and 11, can be fixed at zero to simulate the single-site Langmuir isotherm. According to the chosen model and parameter list the objective function generates the input data for the simulator. This includes calculating the kinetic and

equilibrium parameters at the experimental conditions: the parameters passed to the objective function are at the user defined reference temperature. Thus the Langmuir constants and the effective macropore diffusivity have to be adjusted. The effective macropore diffusivity is calculated by

$$D_p = D_p^0 \left(\frac{T}{T_{ref}} \right)^{1.75} \tag{17}$$

The simulations are run with the given parameters and for each experiment the deviation between the simulation and experiment is calculated by the following expression

$$E = \frac{0.5}{N} \left(\frac{1}{n} \left(\sum_{i=1}^{n} \frac{(s_i - C_i)^2}{s_i^2} \right) + \frac{1}{m-n} \left(\sum_{i=n+1}^{m} \frac{(s_i - C_i)^2}{s_i^2} \right) \right) \tag{18}$$

The two least squares errors characterise the short- and long-time region, respectively. Here m is the total number of data points and n is chosen so that $C_i < 0.007$ for $i > n$. The splitting of the error function is essential to ensure that both the short- and long-time regions are fitted well. For the simultaneous fitting of multiple experiments the individual deviations are averaged.

A hybrid, two stage optimisation strategy is used to minimise the average deviation. In the first stage the genetic algorithm NSGA2 from the Python module *inspyred* [39] is used and in the second stage the Nelder-Mead simplex algorithm from the *scipy* module. Both stages are run for a fixed number of function evaluations. The genetic algorithm uses a population size of 140 and 14 generations; the simplex algorithm uses 300 iterations. These conditions allow the reliable estimation of the parameters (see Section 5). The genetic algorithm searches the parameter space given by the lower and upper bounds shown in Table 1.

Table 1: Lower and upper bound of the parameters used in the global optimisation

Parameter	D_p	D_μ / r_μ^2	q_{s1}	b_1	$-\Delta H_1$	q_{s2}	b_2	$-\Delta H_2$
Unit	$m^2\,s^{-1}$	s^{-1}	mol kg^{-1}	bar^{-1}	J mol^{-1}	mol kg^{-1}	bar^{-1}	J mol^{-1}
Lower bound	10^{-7}	0.01	0.5	0	20 000	0	0	20 000
Upper bound	10^{-5}	10.0	5.0	70	43 000	5.0	200	43 000

4. Estimation of kinetic and isotherm parameters of zeolite 13X

The parameter estimation was tested with ZLC experiments on zeolite 13X pellets (APG MOLSIV™) from UOP, a Honeywell company. The adsorbent parameters relevant to these experiments are given in Table 2.

Table 2: Parameters of the zeolite 13X pellets

Description	**Parameter**	**Value**	**Unit**
Adsorbent mass (dry)	m	13.8	mg
Pellet radius	R	0.001	m
Macropore void fraction	ε_p	0.25	-
Crystal density	ρ_μ	1 404	kg m^{-3}

The experiments are performed at flow rates of 30 cc/min and 40 cc/min and at temperatures of 35 °C and 60 °C. This is a particularly interesting test system since at 10% CO_2 there will be nonlinearities resulting from the adsorption isotherm and given that the system is macropore diffusion controlled there will also be a concentration dependent diffusivity. The traditional approach based on a linear isotherm and a constant diffusivity will provide only an approximate match.
The parameter estimation is performed in two steps. In the first step the parameters of the empty system, i.e. no adsorbent in the ZLC, are fitted with empty system experimental runs. Then in the second step only the kinetic and equilibrium parameters in the ZLC are fitted.

4.1 Fitting of the detector parameters

In the first step the parameters of the detector are fitted with the data from the blank experiment. A good fit of the blank data is essential to remove uncertainty with respect to the dead volume in the lines, the start of the desorption step and the response of the detector with respect to the effluent concentration. For the blank experiments the mass of adsorbent is set to zero and the available data sets are fitted simultaneously. Figure 3 shows the fit of the blank data at 35°C and for both flow rates.

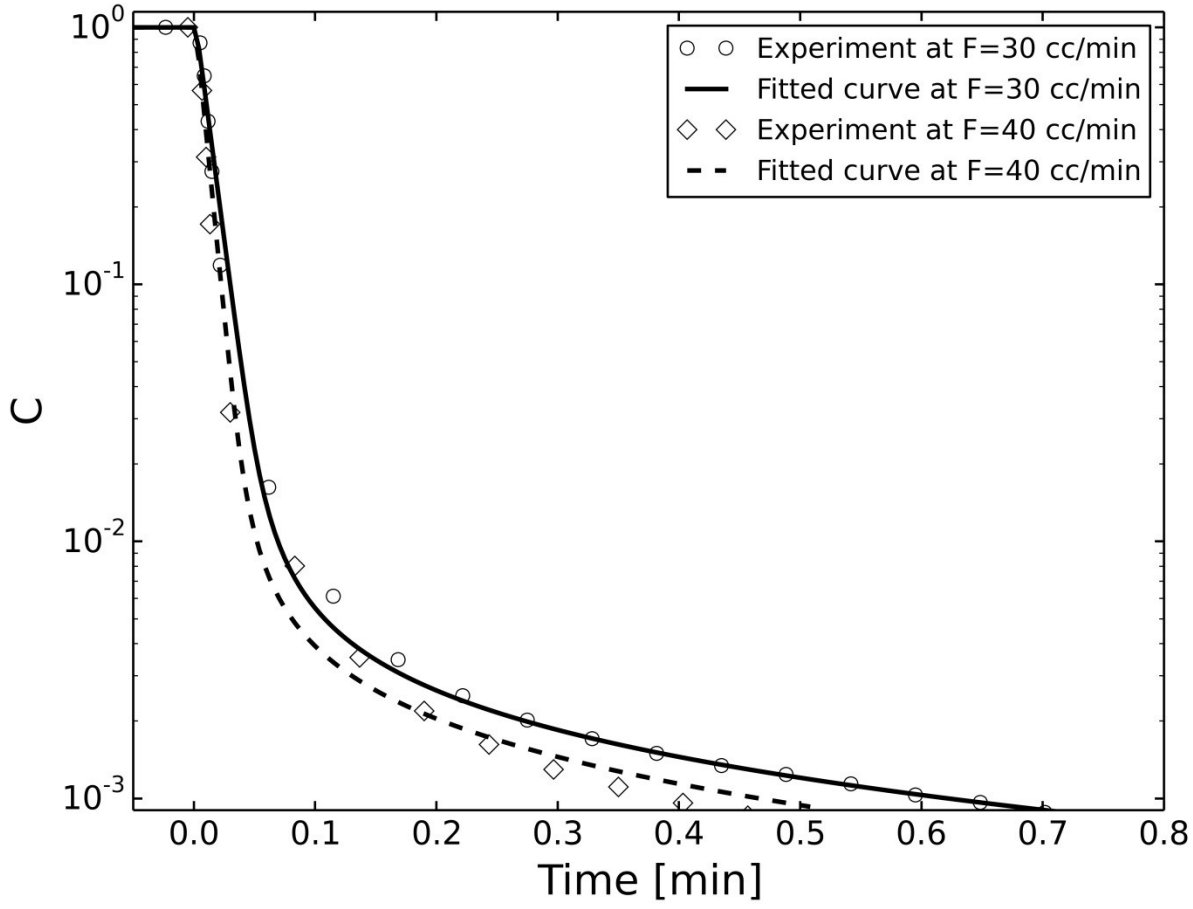

Figure 3: Fit of the blank experimental data for the fast flow rate ZLC system with T=35° C

Both flow rates can be fitted with one set of detector parameters, i.e. LDF mass transfer parameter, the saturation capacity and the equilibrium constant. There is a small discrepancy in the long-time region at relative concentrations of 10^{-3} for the faster flow rate. The good fit for both blank experiments shows that the detector itself is almost independent of the flow rate and gives an indirect confirmation of the chosen detector model; thus the fit of the non-blank experiments can be performed with one set of detector parameters which are given in Table 3.

Table 3: Parameters of the detector

Description	**Parameter**	**Value**	**Unit**
Detector volume	V	$4*10^{-7}$	m^3
Void fraction	ε	0.95	-
LDF mass transfer	k	12.4	s^{-1}
Saturation capacity	q_s	17.5	mol m^{-3}
Equilibrium constant	b	10 878	bar^{-1}

4.2 Fitting of the kinetic and equilibrium parameters

After the detector parameters the non-blank experiments can be examined. The fitting of the long-time asymptote gives an approximated value of $L \approx 100$. Thus the experiments are under kinetic control and the traditional analysis would only be able to estimate kinetics and the adsorbed capacity of CO_2 at 0.1 bar partial pressure. The four experiments, i.e. experiments at two temperatures and two flow rates, are fitted first with the dual-site Langmuir isotherm and then with the single-sit Langmuir isotherm.

For the dual-site Langmuir isotherm 8 parameters (2 kinetic and 6 equilibrium) need to be regressed. The fitted and experimental curves plotted in Figure 4 show very good agreement for all four experiments. The fitted curves are generated from one parameter set thus giving a confident estimation of the kinetic and equilibrium parameters for this sample of zeolite 13X. The fit of the blank data is shown to indicate the time scales of the blank and experimental runs. For 20 runs of the fitting the error given by Eq. 18 is in the range between 1.3 and 3.3; thus the error is 1.3 to 3.3 times the noise in the long-time region.

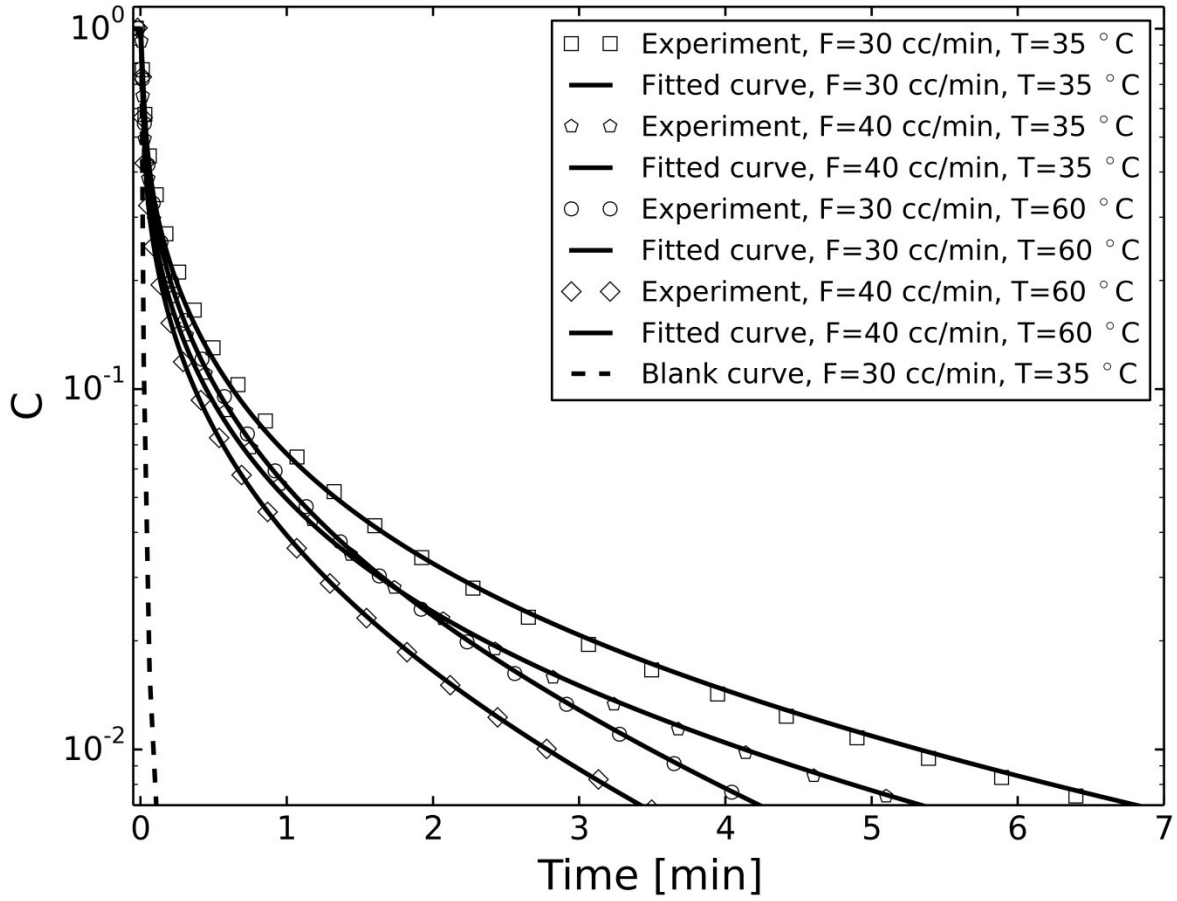

Figure 4: Results for the simultaneous fit of four experimental curves with the dual-site Langmuir isotherm.

For the single-site Langmuir isotherm 5 parameters (2 kinetic and 3 equilibrium) are fitted with the same optimisation procedure (see Section 3.2); see Figure 5. It is clearly evident that the fitting deviates significantly in both the short- and long-time region. The fitting was performed 10 times and the parameters of the single-site Langmuir isotherm varied by less than 1%. However, the value of the error is 17 which is much larger than the error for the dual-site Langmuir fit.

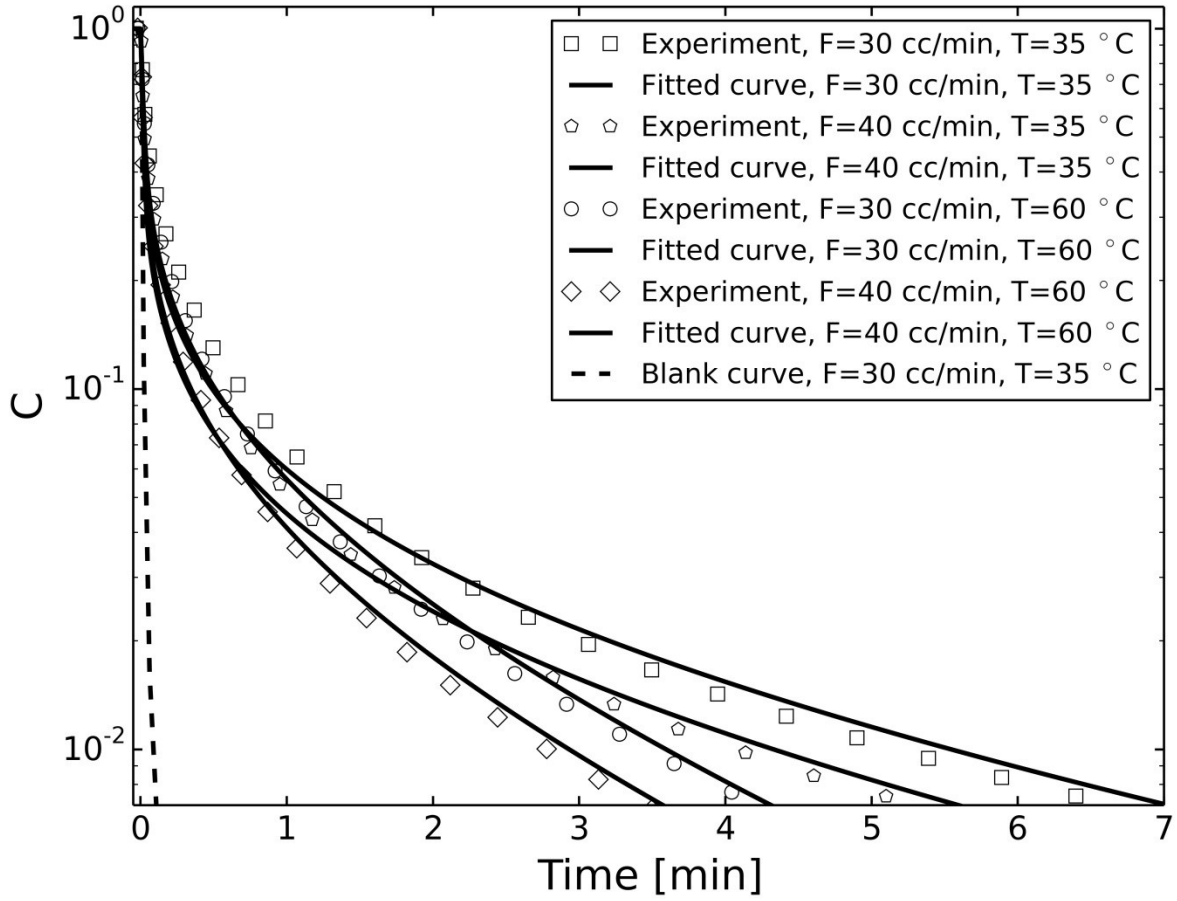

Figure 5: Results for the simultaneous fit of four experimental curves with the single-site Langmuir isotherm.

5. Discussion

Traditionally the fast flow rate ZLC experiments are used to measure the adsorption capacity (from the total area below the desorption curve) and the kinetics (from the long-time asymptote) while the slow flow rate ZLC experiments are used to measure the isotherm [24]. However, with the automated fitting described here a good approximation of the isotherm can be recovered directly from the fast flow rate ZLC in the case of a macropore diffusion controlled system. Figure 6 shows a comparison of the isotherms obtained from 20 runs of the fitting presented in Section 4.2 with the isotherm obtained from slow flow rate ZLC experiments on the same sample and with an isotherm generated on a larger sample (0.47 g) on a Quantachrome Autosorb iQ system.

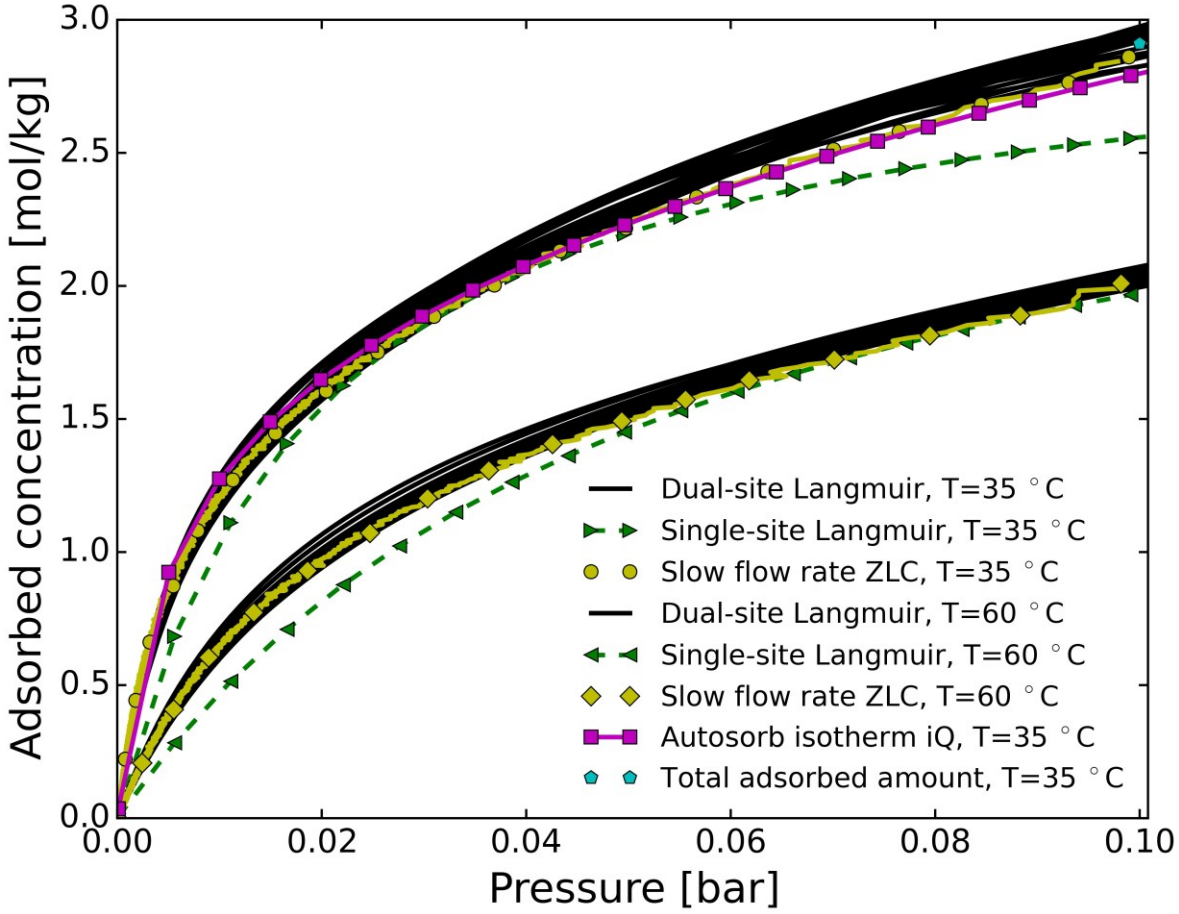

Figure 6: Comparison of the isotherm fitted from the fast flow rate ZLC to the isotherm calculated from the slow flow rate ZLC data and the isotherm from the Quantachrome Autosorb iQ. The black lines show the fitted isotherms for 20 runs of the parameter estimation.

The dual-site Langmuir isotherms obtained from the fast flow rate data in Section 4.2 show good agreement with the independently obtained isotherms. In addition, the total adsorbed amount at 0.1 bar of CO_2 at 35°C is in the range of values reported in the literature [40], [41]. The difference between the Autosorb isotherm is most likely due to a slightly (~4%) above average crystal fraction in the 3 adsorbent pellets used for the ZLC experiment. Furthermore, Figure 6 shows the poor fit of the single-site Langmuir isotherm. This corresponds to the larger error in the fitting (Figure 5). Together this confirms that the Langmuir isotherm cannot accurately describe the CO_2 isotherm on zeolite 13X over the partial pressure range used in the ZLC experiments.

To have a comparison with the analytical method (Section 2.2) the fitting was repeated with a linear isotherm; see Figure 7. The results of this fit show what the analytical solution coupled to a regression algorithm can obtain, i.e. the previous approaches in the literature. While the fit is generally poor, the slope of the long-time region is recovered with reasonable accuracy. This is particularly the case for the higher temperature curves which can be explained by the reduced nonlinearity of the isotherm at higher temperatures. Table 4 shows the Henry's law constants and effective pore diffusivities for the

three different isotherms. While the fits with all isotherms arrive at a similar pore diffusivity, the Henry's law constants vary by one order of magnitude.

Table 4: Comparison between the different isotherms.

Isotherm	**K**	**D**
Linear	830	$5.8*10^{-10}\ m^2\ s^{-1}$
Single-site Langmuir	4235	$4.1*10^{-10}\ m^2\ s^{-1}$
Dual-site Langmuir	7637	$4.2*10^{-10}\ m^2\ s^{-1}$

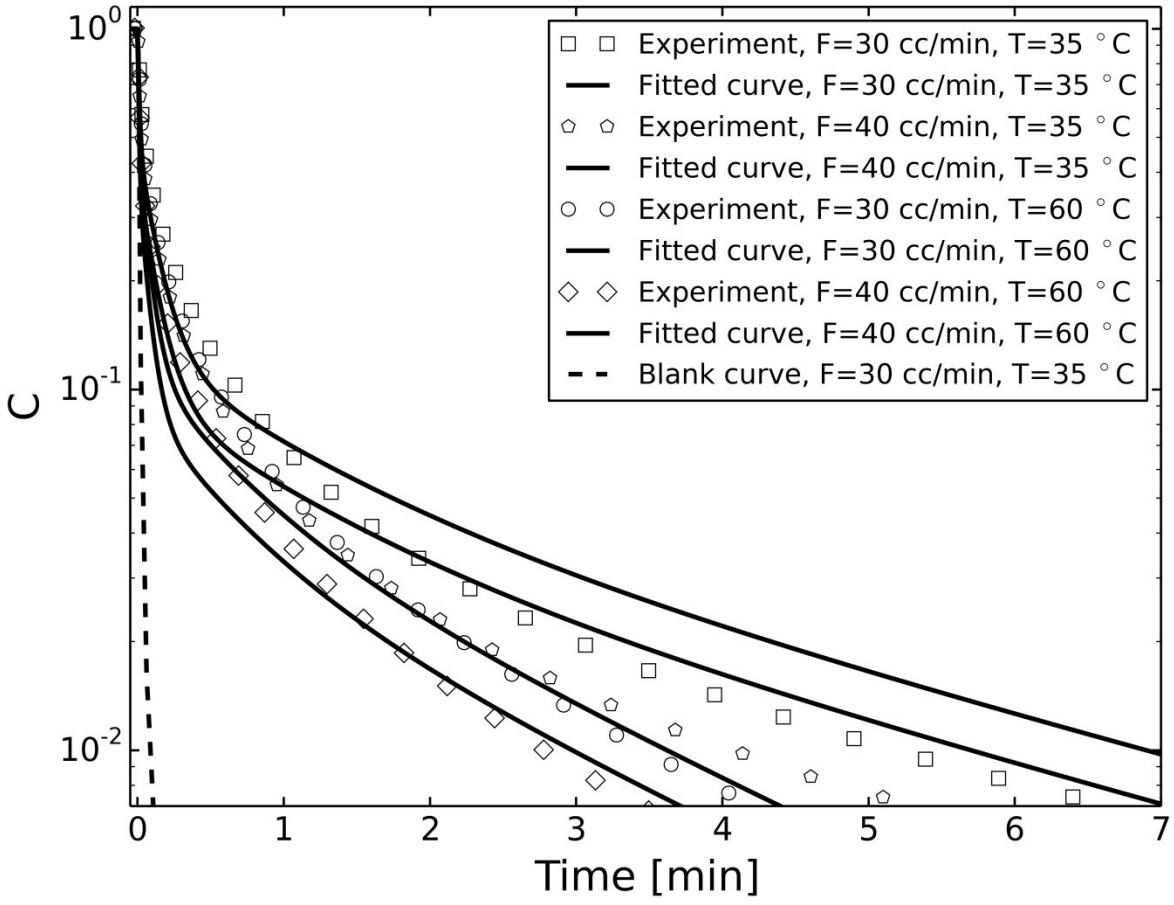

Figure 7: Results for the simultaneous fit of four experimental curves with a linear isotherm.

There is a maximum difference of about 5% between the dual-site Langmuir isotherms of the repeated parameter estimation runs shown in Figure 6. From the high level representation of the fitted parameters shown in Figure 8 for 20 runs of the parameter estimation it can be seen that the dual-site Langmuir isotherm parameters vary considerably between different runs while the resulting isotherms are fairly close. Thus the effect of these variations balances as can be seen by the low variability of the Henry's law constant K. The long-time region of the desorption curve is in the Henry

law region which therefore can be determined with good accuracy. The rest of the isotherm is mainly estimated from the initial part of the curve. The variability in the isotherm is due to the fitting in this high concentration region where variations in the isotherm have a lower impact on the shape of the desorption curve. Therefore, it should be possible to reduce the variability in the isotherm by using the total adsorbed amount calculated in Eq. 15 to constrain the fitting, i.e. require that the isotherm at 0.1 bar is equal to the total adsorbed amount. The total adsorbed amount which is plotted in Figure 6 is in the middle of the range of fitted dual-site Langmuir isotherms. This has the added benefit of reducing the number of parameters and will be investigated in a subsequent publication.

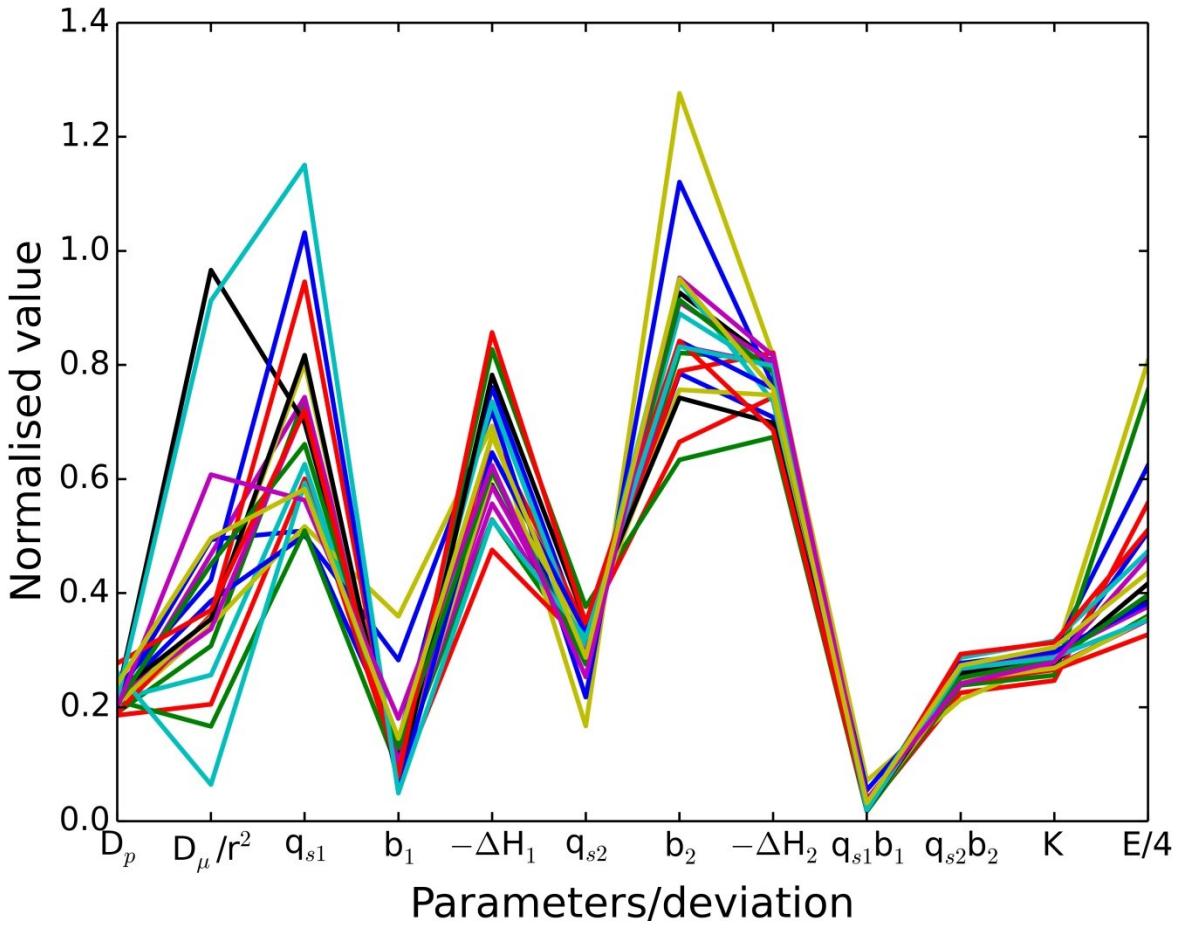

Figure 8: High level representation of the fitted parameters and the deviation for the dual-site Langmuir fit. The parameter K is the normalised Henry's law constant.

The micropore time constant varies considerably over the 20 runs while the effective macropore diffusivity is almost constant; see Figure 8. The micropore time constant varies between 0.65 and 9.66 s^{-1} while the effective macropore diffusivity varies between $1.94*10^{-6}$ and $2.84*10^{-6}$ $m^2\,s^{-1}$. Following the calculation of the Knudsen and molecular diffusion reported in a previous publication [8] this leads to a tortuosity between 2.51 and 3.67. LeVan and co-workers [42] reported a lower effective macropore diffusivity which can be explained by the smaller pore radius of their sample: 32 nm compared to 294 nm for the pellets used in this study. The variation in the micropore time constant suggests that the micropore resistance has no influence on the behaviour of the system which is thus

macropore diffusion controlled. The variation is even more obvious for the single-site Langmuir fit: the micropore time constant varies between 0.67 and 10.51 s^{-1} while the other parameters vary by less than 1%. This supports a previous study which showed that the adsorption of CO_2 on zeolite 13X pellets is macropore diffusion controlled [8].

The variation in the fitted isotherms suggests that it might be beneficial to independently measure the isotherm to get a more accurate estimation of the kinetics. For the system considered in this contribution it is possible to measure independently the adsorption isotherm, but given that the material is composed of crystals and a binder the actual adsorption isotherm of the individual pellets has some variability and one should not expect the isotherms to overlap exactly. If the isotherm from the Autosorb is normalised using the total amount adsorbed calculated from Eq. 15, it is possible to use the automated tool to regress the data to obtain directly the effective diffusivity. In this case the value found is $4.25*10^{-10}$ $m^2 s^{-1}$ which is in excellent agreement with the range obtained directly from the ZLC experiments. If the independent isotherm is not normalised the pore diffusivity obtained is $5.46*10^{-10}$ $m^2 s^{-1}$, which is clearly too high. It is recommended to fit both equilibrium and kinetic parameters directly from the ZLC data, provided that experiments are carried out over a sufficiently broad range of flow rates and temperatures.
Figure 8 shows that for most fitting runs the parameters are within the boundaries used for the global optimisation (see Table 1). However, for 3 runs the saturation capacity or the Langmuir constant are slightly larger than the upper boundary. This is possible due to the unconstrained optimisation in the second step which allows the parameter values to go beyond the given parameter space. As a consequence this might allow a successful fitting, even if the upper and lower bounds were too restrictive, or at least point out a wrong choice of boundaries. The low variation in the governing parameter values and fitting error as well as the absence of outliers shows that the employed hybrid optimisation strategy can reliably and accurately estimate the kinetic and equilibrium parameters from the experimental curves. In contrast, a purely local optimisation strategy with a random starting point was not always successful. Furthermore, the excellent fit of the simulation over the whole range of the desorption curve (see Figure 4) validates the choice of error expression in Eq. 18. The normalisation ensures that all points of the desorption curve have equal weight. In a previous study the unscaled least squares expression was used with the consequence of a poor fit of the long-time region [32] which includes most of information on mass transfer kinetics.

The fitting as described here is applicable to a wide range of adsorbate-adsorbent systems. The only assumptions are that the equilibrium can be described by a dual-site Langmuir isotherm and that the adsorption kinetics can be described by a combination of macropore and micropore diffusion. The fitting of the desorption curves of CO_2 on zeolite 13X were performed with a parameter range which allowed macropore control, micropore control and equilibrium control. By repeating the optimisation it became apparent that the micropore time constant has no effect on the fitting. Due to the reliable convergence of the optimisation routine the comparison of the noise level to the fitting error gives a strong indication of the accuracy of the fitting as well as the resulting isotherm and kinetic resistances. For example, repeating the fitting of section 4.2 with the macropore diffusivity fixed at 10^{-4} $m^2 s^{-1}$ results in an error which is more than an order of magnitude larger than the noise level and thus indicates that the chosen model is not appropriate. For the analysis of an unknown adsorbate-adsorbent system it is important to repeat the parameter estimation and to monitor the fitting error as well as the resulting parameter values. The latter can indicate if the original parameter range was too restrictive.

6. Conclusion

Here a robust, automated tool for the estimation of kinetic and equilibrium parameters from ZLC desorption curves is presented. The parameters are estimated through simultaneous fitting of several experimental curves with different flow rates and temperatures. This increases the robustness of the parameter estimation as well as the confidence in the results. For the correct choice of models the deviation between the experiments and simulations reaches almost the noise level of the experimental data; showing that the simulator can provide an accurate description of the dynamics of the ZLC system. Indeed, if the deviation between the experiments and simulations is close to the noise level the estimated parameters agree with results from independent experiments. This was demonstrated with experiments performed with zeolite 13X pellets, which are an example of an adsorbent with macropore diffusion control with a nonlinear isotherm, i.e. variable diffusional time constant. Furthermore, the developed tool not only correctly estimated the kinetic parameters but also the isotherm parameters from kinetically controlled data. To achieve this with the traditional analysis of ZLC experiments would require experimental data both in the kinetically and the equilibrium controlled regime. Here the isotherm is estimated with a variability of around 5% which is mostly in the high concentration region. The variability might be reduced by using a lower range mass flow controller or by constraining the fitting with the total adsorbed amount: these will be investigated in a future contribution.

The employed hybrid optimisation scheme utilising a global optimisation in the first stage and a local optimisation in the second stage is crucial for the good performance of the parameter estimation. The first stage ensures that the correct region of the parameter space is found while the second stage has a faster convergence to a minimum. Scope for an improvement in the computational time lies in the integration of a stopping criterion based on the noise level.

The tool utilises a sophisticated adsorption simulator to simulate the ZLC, the detector and the surrounding units. Thus the dynamics of the piping and the detector are explicitly included which reduces the uncertainty in the analysis of the experiments. Furthermore, since the parameters are fitted with a full-scale column model they can be used immediately in simulations of further adsorption processes without rescaling or conversion. In addition to this, the flexibility of the adsorption simulator, i.e. different kinetic and equilibrium models, allows investigating which of these models are applicable. Here it was shown that fits with the dual-site Langmuir isotherm reach deviations very close to the noise level while fits with the single-site Langmuir isotherm have deviations at least an order of magnitude larger; confirming that the single-site Langmuir isotherm can't accurately describe the adsorption of CO_2 on zeolite 13X. In a future contribution the fitting tool will be extend to include capabilities to investigate the dominating mass transfer mechanisms and to check the validity of the momentum and energy balance assumptions.

Notation

b_i	Equilibrium constant, bar^{-1}
c	Gas phase concentration, mol m^{-3}
c_0	Initial gas phase concentration, mol m^{-3}

c^m	Macropore gas phase concentration, mol m^{-3}
C	Normalised gas phase concentration
D	Effective pore diffusivity, $m^2 s^{-1}$
D_p	Effective macropore diffusivity, $m^2 s^{-1}$
D_μ	Micropore diffusivity, $m^2 s^{-1}$
E	Deviation between experiment and simulation
F	Flow rate, $m^3 s^{-1}$
$-\Delta H_i$	Heat of adsorption, J mol^{-1}
J	Diffusive flux in the fluid phase, mol $m^{-2} s^{-1}$
k	LDF mass transfer parameter, s^{-1}
K	Henry's law constant
L	Ratio of the diffusional and convective time constant
N	Noise level of the experimental data
P	Pressure, bar
q	Sorbate concentration, mol m^{-3}
q^*	Sorbate concentration at equilibrium, mol m^{-3}
q_{si}	Saturation capacity, mol m^{-3}
Q	Concentration in the pellet, mol m^{-3}
$\overline{Q}$	Average concentration in the pellet, mol m^{-3}
r_μ	Crystal radius, m
R	Pellet radius, m
s_i	Simulated desorption curve
t	Time, s
T	Temperature, K
v	Interstitial flow velocity, m s^{-1}
V	Detector volume, m^3
V_g	Gas volume, m^3
V_s	Solid volume, m^3
y	Mole fraction
z	Axial dimension, m

Greek letters

β_n	Nondimensional parameters in Eq. 2
γ	Ratio of fluid volume and accumulation in the solid
ε	Bed void fraction
ε_p	Macropore void fraction
σ	Raw experimental data

Acknowledgements

Financial support from the EPSRC through Grants EP/I010939/1 and EP/J02077X/1 is gratefully acknowledged.

References

[1] M. Eic and D. M. Ruthven, “A new experimental technique for measurement of intracrystalline diffusivity,” *Zeolites*, vol. 8, pp. 40–45, 1988.

[2] P. Grenier, F. Meunier, P. G. Gray, J. Kärger, Z. Xu, and D. M. Ruthven, “Diffusion of methanol in NaX crystals: Comparison of i.r., ZLC, and PFG-n.m.r. measurements,” *Zeolites*, vol. 14, pp. 242–249, Apr. 1994.

[3] M. Eic, M. Goddard, and D. M. Ruthven, “Diffusion of benzene in NaX and natural faujasite,” *Zeolites*, vol. 8, pp. 327–331, 1988.

[4] C. L. Cavalcante Jr, M. Eic, D. M. Ruthven, and M. L. Occelli, “Diffusion of n-paraffins in offretite-erionite type zeolites,” *Zeolites*, vol. 15, pp. 293–307, 1995.

[5] M. Eic and D. M. Ruthven, “Diffusion of linear paraffins and cyclohexane in NaX and 5A zeolite crystals,” *Zeolites*, vol. 8, pp. 472–479, 1988.

[6] J. R. Hufton and D. M. Ruthven, “Diffusion of light alkanes in silicalite studied by the zero length column method,” *Ind. Eng. Chem. Res.*, vol. 32, pp. 2379–2386, Oct. 1993.

[7] D. M. Ruthven and Z. Xu, “Diffusion of oxygen and nitrogen in 5A zeolite crystals and commercial 5A pellets,” *Chem. Eng. Sci.*, vol. 48, no. 18, pp. 3307–3312, 1993.

[8] X. Hu, E. Mangano, D. Friedrich, H. Ahn, and S. Brandani, “Diffusion mechanism of CO2 in 13X zeolite beads,” *Adsorption*, vol. 20, no. 1, pp. 121–135, Jun. 2014.

[9] A. Vidoni and D. M. Ruthven, “Diffusion of C2H6 and C2H4 in DDR Zeolite,” *Ind. Eng. Chem. Res.*, vol. 51, pp. 1383–1390, Jan. 2012.

[10] D. M. Ruthven and A. Vidoni, “ZLC diffusion measurements: Combined effect of surface resistance and internal diffusion,” *Chem. Eng. Sci.*, vol. 71, pp. 1–4, Mar. 2012.

[11] D. Ruthven and F. Brandani, “ZLC Response for Systems with Surface Resistance Control,” *Adsorption*, vol. 11, no. 1, pp. 31–34, Jan. 2005.

[12] S. Brandani, J. Hufton, and D. M. Ruthven, “Self-diffusion of propane and propylene in 5A and 13X zeolite crystals studied by the tracer ZLC method,” *Zeolites*, vol. 15, pp. 624–631, Oct. 1995.

[13] S. Brandani and D. M. Ruthven, “Concentration dependence of self-diffusivity of methanol in NaX zeolite crystals,” *Zeolites*, vol. 15, pp. 494–495, 1995.

[14] S. Brandani, M. Jama, and D. M. Ruthven, “Diffusion, self-diffusion and counter-diffusion of benzene and p-xylene in silicalite,” *Microporous Mesoporous Mater.*, vol. 35–36, pp. 283–300, 2000.

[15] D. M. Ruthven and P. Stapleton, “Measurement of liquid phase counter-diffusion in zeolite crystals by the ZLC method,” *Chem. Eng. Sci.*, vol. 48, no. 1, pp. 89–98, Jan. 1993.

[16] S. Brandani and D. M. Ruthven, “Analysis of ZLC desorption curves for gaseous systems,” *Adsorption*, vol. 2, no. 2, pp. 133–143, 1996.

[17] A. Gunadi and S. Brandani, “Diffusion of linear paraffins in NaCaA studied by the ZLC method,” *Microporous Mesoporous Mater.*, vol. 90, pp. 278–283, 2006.

[18] S. Brandani and D. M. Ruthven, “Analysis of ZLC Desorption Curves for Liquid Systems,” *Chem. Eng. Sci.*, vol. 50, no. 13, pp. 2055–2059, Aug. 1995.

[19] S. Brandani, “Effects of nonlinear equilibrium on zero length column experiments,” *Chem. Eng. Sci.*, vol. 53, no. 15, pp. 2791–2798, Aug. 1998.

[20] S. Brandani, M. A. Jama, and D. M. Ruthven, “ZLC Measurements under non-linear conditions,” *Chem. Eng. Sci.*, vol. 55, pp. 1205–1212, 2000.

[21] S. Brandani, C. Cavalcante, A. Guimaraes, and D. M. Ruthven, “Heat Effects in ZLC Experiments,” *Adsorption*, vol. 4, pp. 275–285, 1998.

[22] S. Brandani, “Analytical solution for ZLC desorption curves with bi-porous adsorbent particles,” *Chem. Eng. Sci.*, vol. 51, no. 12, pp. 3283–3288, 1996.

[23] W. L. Duncan and K. P. Moller, “The effect of a crystal size distribution on ZLC experiments,” *Chem. Eng. Sci.*, vol. 57, pp. 2641–2652, 2002.

[24] F. Brandani, D. M. Ruthven, and C. G. Coe, “Measurement of Adsorption Equilibrium by the Zero Length Column (ZLC) Technique Part 1: Single-Component Systems,” *Ind. Eng. Chem. Res.*, vol. 42, pp. 1451–1461, Apr. 2003.

[25] F. Brandani and D. Ruthven, “Measurement of Adsorption Equilibria by the Zero Length Column (ZLC) Technique Part 2: Binary Systems,” *Ind. Eng. Chem. Res.*, vol. 42, pp. 1462–1469, Apr. 2003.

[26] E. Mangano, S. Brandani, M.-C. Ferrari, H. Ahn, D. Friedrich, M. L. Lozinska, P. a. Wright, J. Kahr, R. Morris, M. Croad, N. McKeown, H. Shamsipour, and P. Budd, “Efficient and rapid screening of novel adsorbents for carbon capture in the UK IGSCC project,” *Energy Procedia*, vol. 37, pp. 40–47, Jan. 2013.

[27] E. Mangano, S. Brandani, and D. M. Ruthven, “Analysis and Interpretation of Zero Length Column Response Curves,” *Chemie Ing. Tech.*, vol. 85, no. 11, pp. 1714–1718, Nov. 2013.

[28] A. Micke, M. Kočiřik, and M. Bülow, “Theory of zero length column chromatography with the condition of a well-stirred sorbing zone,” *Microporous Mater.*, vol. 1, pp. 363–371, 1993.

[29] A. Micke, M. Kočiřik, and M. Bülow, “Zero length column chromatography to characterise microporous sorbents bey means of kinetic data,” *Berichte der Bunsengesellschaft für Phys. Chemie*, vol. 98, pp. 242–248, 1994.

[30] F. Brandani, A. Rouse, S. Brandani, and D. M. Ruthven, “Adsorption Kinetics and Dynamic Behavior of a Carbon Monolith,” *Adsorption*, vol. 10, pp. 99–109, Jun. 2004.

[31] J.-B. W. P. Loos, P. J. T. Verheijen, and J. A. Moulijn, “Improved estimation of zeolite diffusion coefficients from zero-length column experiments,” *Chem. Eng. Sci.*, vol. 55, pp. 51–65, 2000.

[32] M. Han, X. Yin, Y. Jin, and S. Chen, “Diffusion of aromatic hydrocarbon in ZSM-5 studied by the improved zero length column method,” *Ind. Eng. Chem. Res.*, vol. 38, pp. 3172–3175, 1999.

[33] D. M. Ruthven, S. Brandani, and M. Eic, “Measurement of Diffusion in Microporous Solids by Macroscopic Methods,” in *Molecular Sieves*, no. December 2005, 2008, pp. 45–84.

[34] D. Friedrich, M.-C. Ferrari, and S. Brandani, “Efficient simulation and acceleration of convergence for a Dual Piston Pressure Swing Adsorption system,” *Ind. Eng. Chem. Res.*, vol. 52, pp. 8897–8905, 2013.

[35] W. Dang, D. Friedrich, and S. Brandani, “Characterisation of an automated Dual Piston Pressure Swing Adsorption (DP-PSA) system,” *Energy Procedia*, vol. 37, pp. 57–64, Jan. 2013.

[36] A.-M. Banu, D. Friedrich, S. Brandani, and T. Düren, “A multiscale study of MOFs as adsorbents in H2 PSA purification,” *Ind. Eng. Chem. Res.*, vol. 52, pp. 9946–9957, 2013.

[37] M. Luberti, D. Friedrich, S. Brandani, and H. Ahn, “Design of a H2 PSA for cogeneration of ultrapure hydrogen and power at an advanced Integrated Gasification Combined Cycle with pre-combustion capture,” *Adsorption*, vol. 20, no. 2, pp. 511–524, 2014.

[38] H. Wang, S. Brandani, G. Lin, and X. Hu, “Flowrate correction for the determination of isotherms and Darken thermodynamic factors from Zero Length Column (ZLC) experiments,” *Adsorption*, vol. 17, pp. 687–694, Aug. 2011.

[39] “inspyred: Bio-inspired Algorithms in Python.” [Online]. Available: http://inspyred.github.io/.

[40] Y. Wang and M. D. LeVan, “Adsorption Equilibrium of Carbon Dioxide and Water Vapor on Zeolites 5A and 13X and Silica Gel: Pure Components,” *J. Chem. Eng. Data*, vol. 54, no. 10, pp. 2839–2844, Oct. 2009.

[41] D. Ferreira, R. Magalhaes, P. Taveira, and A. Mendes, “Effective Adsorption Equilibrium Isotherms and Breakthroughs of Water Vapor and Carbon Dioxide on Different Adsorbents,” *Ind. Eng. Chem. Res.*, vol. 50, pp. 10201–10210, 2011.

[42] T. J. Giesy, Y. Wang, and M. D. LeVan, “Measurement of Mass Transfer Rates in Adsorbents: New Combined-Technique Frequency Response Apparatus and Application to CO 2 in 13X Zeolite,” *Ind. Eng. Chem. Res.*, vol. 51, no. 35, pp. 11509–11517, Sep. 2012.